

Wave mechanics and the adhesion approximation

C J Short and P Coles

Cripps Centre for Astronomy and Particle Theory, School of Physics and Astronomy,
University of Nottingham, University Park, Nottingham, UK, NG7 2RD

E-mail: ppxcjs@nottingham.ac.uk, peter.coles@nottingham.ac.uk

Abstract. The dynamical equations describing the evolution of a self-gravitating fluid of cold dark matter (CDM) can be written in the form of a Schrödinger equation coupled to a Poisson equation describing Newtonian gravity. It has recently been shown that, in the quasi-linear regime, the Schrödinger equation can be reduced to the exactly solvable free-particle Schrödinger equation. The free-particle Schrödinger equation forms the basis of a new approximation scheme -the *free-particle approximation* - that is capable of evolving cosmological density perturbations into the quasi-linear regime. The free-particle approximation is essentially an alternative to the adhesion model in which the artificial viscosity term in Burgers' equation is replaced by a non-linear term known as the *quantum pressure*. Simple one-dimensional tests of the free-particle method have yielded encouraging results. In this paper we comprehensively test the free-particle approximation in a more cosmologically relevant scenario by appealing to an N -body simulation. We compare our results with those obtained from two established methods: the linearized fluid approach and the Zeldovich approximation. We find that the free-particle approximation comprehensively out-performs both of these approximation schemes in all tests carried out and thus provides another useful analytical tool for studying structure formation on cosmological scales.

PACS numbers: 95.35.+d, 98.65.Dx, 98.80.-k

Submitted to: *J. Cosmol. Astropart. Phys.*

1. Introduction

Over the last two decades a vigorous interplay between theory and observation has led to the establishment of a standard cosmological model that not only describes the composition and evolution of the universe as a whole, but has also scored great successes in accounting for the large-scale structures observed in the universe; for a recent review see, for example, [1]. In this standard model, large-scale structure is thought to be the result of the gravitational amplification of small density perturbations present in the early universe; a mechanism known as gravitational instability. The gravitational instability process is relatively easy to understand at a qualitative level because it mostly relies only on the action of gravity, with more complex hydrodynamical and radiative effects playing a role only at late times when structure is already largely developed.

Moreover, when the density fluctuations are very much smaller than the average density, the growth of fluctuations can be handled quite accurately using first-order (linear) perturbative techniques. On the other hand, galaxies and galaxy clusters represent density enhancements well in excess of the mean density so we need to go beyond linear theory if we are to study the formation of such objects in detail.

The non-linear regime of gravitational instability is analytically intractable, except in a few cases where some special symmetry applies. For the most part, therefore, cosmologists have been forced to resort to numerical methods based on N -body computations in order to study the late stages of the evolution of density fluctuations. The use of computer simulations has revolutionized cosmology, especially in enabling the simulation of the large-scale structure expected to be found in galaxy redshift surveys and the consequent testing of models using observations. In some cases, however, such as when a very large volume and/or very high resolution is needed, one has to make more detailed predictions than can be obtained by using computational techniques. In such cases numerous analytical approximations have been suggested that provide robust results in a necessarily limited range of circumstances (e.g. see [2, 3] and references therein). These approximate techniques also help to promote a genuine understanding of the principal processes involved in the formation of cosmological structure.

Analytical attempts to understand large-scale structure formation are commonly based on the assumption that cold dark matter (CDM) can be treated as a self-gravitating pressureless fluid. Two important approximation methods can be derived from the equations of motion for this fluid by applying linear Eulerian and Lagrangian perturbation theory, respectively. First-order Eulerian perturbation theory - the so-called *linearized fluid approach* (e.g. [4]) - has been the backbone of structure formation theory for many years as a result of its simplicity and robustness at early times/on large scales. However, for Gaussian initial conditions, it generically leads to unphysical regions where the matter density is negative if extrapolated to late times/small scales. Although popular, the linearized fluid approach is considerably less powerful than its Lagrangian counterpart - the *Zeldovich approximation* [5]. The Zeldovich approximation considers (linear) perturbations in the trajectories of individual fluid elements (particles), rather than in macroscopic fluid quantities such as the density field. This technique is remarkably successful in describing the pattern of structure formed from realistic (random) initial conditions (e.g. [6]), as long as care is taken to ensure that particle trajectories do not intersect. Once trajectories cross (a phenomenon known as *shell-crossing*), the velocity field becomes multi-valued and the density field develops a singularity (known as a *caustic*). However, since the Zeldovich approximation is kinematical, particles do not respond to the strong gravitational forces acting in the vicinity of the caustic. Instead they simply continue to move along their original inertial trajectories and any structure formed is rapidly ‘smeared out’ in an unrealistic manner. An alternative to the Zeldovich approximation which avoids this problem is the adhesion model [7], an *ad hoc* extension of the Zeldovich approximation in which particles are assumed to ‘stick’ to each other when shell-crossing occurs. This sticking is achieved by

including an artificial viscosity term in the usual hydrodynamical equations of motion, thus transforming the momentum equation into *Burgers' equation*. The viscous term becomes large when particle trajectories intersect, cancelling the component of the particle velocities perpendicular to the caustic. This prevents particles from simply sailing through the caustic and, consequently, the density singularities predicted by the Zeldovich approximation are regularized and stable structures are formed. Comparisons with N -body simulations have shown that the adhesion model is capable of accurately reproducing the skeleton of the ‘cosmic web’ of filaments and voids that comprises the morphology of the large-scale galaxy distribution [8, 9, 10, 11, 12]. Although the original motivation for the adhesion approximation was purely phenomenological, it has recently been shown that Burgers’ equation can be naturally derived from the coarse-grained equations of motion, provided certain simplifying assumptions are made [13, 14, 15, 16, 17].

A novel alternative approach to the study of large-scale structure formation was suggested by Widrow and Kaiser [18]. They proposed a wave-mechanical description of self-gravitating matter in which collisionless CDM is modelled by a complex scalar field whose dynamics are governed by coupled Schrödinger and Poisson equations (see [19] for a relativistic extension of the original theory). As pointed out by Coles [20], the (approximately) log-normal form of the distribution function of density perturbations can be naturally explained within this wave-mechanical formalism. By appealing to simple one-dimensional examples of gravitational collapse in a static universe, Coles and Spencer [21] showed that the wave-mechanical approach offers a competitive alternative to the Zeldovich approximation, provided the effective Planck constant ν in the theory is chosen carefully. They also demonstrated that, unlike the Zeldovich approximation, the wave-mechanical approach leads to a density field that remains non-singular when shell-crossing occurs. Building on the work of Coles and Spencer, Short and Coles [22] recently showed that, in an expanding universe, the Schrödinger equation can be conveniently reduced to the free-particle Schrödinger equation in the linear and quasi-linear regimes of gravitational instability. They advocated using the free-particle Schrödinger equation as the basis of a new approximation scheme - the *free-particle approximation*. The free-particle approximation is essentially an alternative to the adhesion model in which the viscosity term is replaced by a non-linear term known as the *quantum pressure*; it is this term that prevents the formation of caustics. A convenient property of the free-particle Schrödinger equation is that, like Burgers’ equation, it possesses an analytic solution. Short and Coles [22] used the free-particle method to follow the gravitational evolution of a plane-symmetric sinusoidal density fluctuation until shell-crossing. By considering such a simple example they were able to carefully elucidate the effect of the quantum pressure term. It was found that, if not properly controlled, the quantum pressure term significantly impedes the growth of density perturbations. However, in the case where the effect of this unusual term was minimized, the free-particle approximation provided an excellent match to the Zeldovich approximation (which is exact in one-dimension up until particle trajectories intersect) and was capable of generating large (non-linear)

over-densities. Our objective in this paper is to provide the first comprehensive test of this promising new method in a cosmologically relevant scenario by appealing to a full N -body simulation. We also assess the performance of the free-particle approximation relative to the established linearized fluid approach and the Zeldovich approximation.

The layout of the paper is as follows: In section 2 we present the central equations of the free-particle approximation and comment on the link between the free-particle, adhesion and Zeldovich approximations. The essentials of the practical implementation of the free-particle method are discussed in section 3. In section 4 we describe the results of our comparison of the free-particle approximation with an N -body simulation. We draw our conclusions in section 5.

2. The free-particle approximation

In the free-particle approximation, collisionless CDM is represented by a complex scalar field $\psi = \psi(\mathbf{x}, D)$ obeying the free-particle Schrödinger equation

$$i\nu \frac{\partial \psi}{\partial D} = -\frac{\nu^2}{2} \nabla_{\mathbf{x}}^2 \psi, \quad (1)$$

where the amplitude and phase of the wavefunction are related via

$$\nu \nabla_{\mathbf{x}}^2 [\arg(\psi)] + \frac{1}{D} (|\psi|^2 - 1) = 0, \quad (2)$$

and the effective Planck constant ν is a free (real) parameter with dimensions of L^2 . For a full derivation of these equations and a discussion of the validity of the free-particle approximation, we refer the reader to [22]. The spatial coordinates $\mathbf{x} = \mathbf{x}(D)$ are comoving coordinates and we use the linear growth factor $D = D(t)$ as a ‘time’ variable, rather than cosmological proper time t . The linear growth factor is the growing mode solution of the differential equation

$$\ddot{D} + 2H\dot{D} - 4\pi G\rho_{b,c}D = 0, \quad (3)$$

where a dot denotes a derivative with respect to t and, at some initial time t_i , $D_i = D(t_i) = 1$. The Hubble parameter $H = H(t)$ is defined by $H \equiv \dot{a}/a$, where the scale factor $a = a(t)$ is normalized to unity at the present epoch, and $\rho_{b,c} = \rho_{b,c}(t)$ is the density of CDM in a homogeneous Friedmann-Robertson-Walker background cosmology. The wavefunction ψ is assumed to be of the *Madelung form* [23]

$$\psi = (1 + \delta)^{1/2} \exp\left(\frac{-i\phi}{\nu}\right), \quad (4)$$

where the density contrast $\delta = \delta(\mathbf{x}, D)$ is defined by $\delta \equiv \rho/\rho_{b,c} - 1$ and describes fluctuations in the CDM density field $\rho = \rho(\mathbf{x}, D)$ about the homogeneous background value $\rho_{b,c}$. The gradient of the velocity potential $\phi = \phi(\mathbf{x}, D)$ gives the comoving velocity field $\mathbf{u} = \mathbf{u}(\mathbf{x}, D)$, defined by $\mathbf{u} \equiv d\mathbf{x}/dD$. Inserting the Madelung transformation (4) into (1) and (2) yields

$$\frac{\partial\phi}{\partial D} - \frac{1}{2} |\nabla_{\mathbf{x}}\phi|^2 + \mathcal{P} = 0, \quad (5)$$

$$\frac{\partial\delta}{\partial D} - \nabla_{\mathbf{x}} \cdot [(1 + \delta)\nabla_{\mathbf{x}}\phi] = 0, \quad (6)$$

and

$$\delta = D\nabla_{\mathbf{x}}^2\phi, \quad (7)$$

respectively. The term $\mathcal{P} = \mathcal{P}(\mathbf{x}, D)$ is known as the quantum pressure term and is given by

$$\mathcal{P} = \frac{\nu^2}{2} \frac{\nabla_{\mathbf{x}}^2 [(1 + \delta)^{1/2}]}{(1 + \delta)^{1/2}}. \quad (8)$$

The link between the free-particle approximation and the more conventional Zeldovich and adhesion approximations becomes apparent upon inspecting the Bernoulli-like equation (5). If we were to set $\mathcal{P} \equiv 0$ then (5) reduces to the so-called *Zeldovich-Bernoulli* equation [24] which, along with the relation (7), arises when the Zeldovich approximation is expressed in Eulerian, rather than Lagrangian, space. On the other hand, replacing \mathcal{P} by a term of the form $\mu\nabla_{\mathbf{x}}^2\phi$ leads to Burgers' equation [25] for the case of an irrotational velocity field; this is the defining equation of the adhesion model (e.g. [7]). The term $\mu\nabla_{\mathbf{x}}^2\phi$ prevents the formation of multi-stream regions and regularizes the density singularities predicted by the Zeldovich approximation. It is controlled by the (real) parameter μ which formally plays the role of a viscosity coefficient in the adhesion approximation. The growth of density perturbations is suppressed on scales $\lesssim \mu^{1/2}$ by the viscous term and thus, for large values of μ , the adhesion model leads to a much smoother distribution of matter than observed in N -body simulations (e.g. [9]). In order to maximize the dynamic range of the adhesion approximation, the (inviscid) limit $\mu \rightarrow 0$ is commonly employed (e.g. [7, 8, 11, 26]). In this limit, the adhesion model reduces exactly to the Zeldovich approximation away from regions where particle trajectories intersect. In modern approximation methods (such as the Euler-Jeans-Newton model [13] and the small-size expansion [15, 16]) where Burgers' equation is consistently *derived* (rather than *assumed*), the constant viscosity coefficient μ is replaced by a density-dependent *gravitational multi-stream coefficient* (see [17] and references therein for a detailed discussion).

The quantum pressure term \mathcal{P} cannot be written in a form proportional to $\nabla_{\mathbf{x}}^2\phi$ and so the free-particle and adhesion approximations are not equivalent. However, the quantum pressure term does play a qualitatively similar role to the viscous term in the sense that it is also a regularizing term, preventing the formation of multi-stream regions and caustics. This was demonstrated by Coles and Spencer [21] who used the Schrödinger equation to follow the evolution of a one-dimensional sinusoidal density fluctuation beyond shell-crossing. The parameter ν controls the quantum pressure term in the same way that μ controls the viscous term and, like μ , ν can

also be viewed as an approximation to a general gravitational multi-stream coefficient. Short and Coles [22] showed that, in the semi-classical limit $\nu \rightarrow 0$, the free-particle approximation reduces exactly to the Zeldovich approximation prior to shell-crossing. The quantum pressure term then only becomes important in regions where particle trajectories intersect. However, for finite ν , the quantum pressure term has an effect before shell-crossing occurs and acts to inhibit the gravitational collapse of density perturbations. The larger the value of ν , the greater the suppression effect; see [22] for a discussion. The free-particle approximation is then no longer identical to the Zeldovich approximation, although they may become similar at a certain distance from collapsing regions, depending on the actual value of ν . Also, once shell-crossing occurs, the quantum pressure term has an effect outside of multi-stream regions in the finite ν case (cf. figure 1 of [21]).

3. Testing the free-particle approximation

In modern cosmology the process of large-scale structure formation is almost exclusively studied using numerical N -body methods since these techniques allow the gravitational evolution of density perturbations to be followed far into the non-linear regime. This is something that cannot be done with any analytical approximation. As a result, N -body simulations provide an ideal tool for testing the applicability of analytical approximation schemes. In this paper we test the free-particle approximation, the linearized fluid approach and the Zeldovich approximation in Eulerian space (which we henceforth refer to as the Zeldovich-Bernoulli approximation) against an N -body simulation so that we may assess the performance of the new free-particle approximation relative to existing methods.

3.1. The N -body simulation

The adaptive P³M code HYDRA [27] was used to perform an N -body simulation. The simulation consisted of $N = 128^3$ CDM particles contained within a cubic box of comoving side length $L = 200h^{-1}$ Mpc equipped with periodic boundary conditions. Here h is the present value of the Hubble parameter H_0 in units of $100 \text{ km s}^{-1} \text{ Mpc}^{-1}$. A spatially-flat Λ CDM cosmological model was assumed with parameters $\Omega_{c,0} = 0.24$, $\Omega_{b,0} = 0$, $\Omega_{\Lambda,0} = 0.76$, $h = 0.73$ where $\Omega_{c,0}$, $\Omega_{b,0}$ and $\Omega_{\Lambda,0}$ are the present values of the CDM, baryon and dark energy density parameters, respectively. The simulation began at an initial scale factor $a_i = 0.02$ and the particles were initially positioned so as to form a random realization of a CDM density field with a power spectrum $P = P(k)$ of the form:

$$P = T^2 P_i, \tag{9}$$

where $P_i = P_i(k)$ is the primordial power spectrum of density fluctuations generated by inflation and $T = T(k)$ is the transfer function. We assume that the primordial power spectrum is scale-invariant: $P_i \propto k$, as predicted by a general class of inflationary

models (see, for example, [28] for a review). The following empirical form for the CDM transfer function was adopted [29]:

$$T = \frac{\ln(1 + 2.34q)}{2.34q} [1 + 3.89q + (16.1q)^2 + (5.46q)^3 + (6.71q)^4]^{-1/4}, \quad (10)$$

where $q = q(k)$ is given by $q = k\theta^{1/2}/(\Omega_{c,0}h^2 \text{ Mpc}^{-1})$ and $\theta = \kappa/1.68$. Here $\kappa = \Omega_{r,0}/\Omega_{\gamma,0}$ is the ratio of the present relativistic particle and photon density parameters respectively; in a universe with three relativistic neutrino flavours and photons $\kappa = 1.68$. Finally, the power spectrum was normalized so that the present value of the rms density fluctuation in spheres of radius $8h^{-1} \text{ Mpc}$ ($\sigma_{8,0}$) was 0.74. The Newtonian gravitational evolution of the CDM distribution was then followed from $a_i = 0.02$ to the present $a_0 = 1$, with the comoving positions of all N particles stored at 20 different output values of the scale factor.

3.2. The testing process

To test the Eulerian free-particle, linearized fluid and Zeldovich-Bernoulli approximations against the Lagrangian N -body simulation described above, we divide the cubic simulation volume (of comoving side length $L = 200h^{-1} \text{ Mpc}$) into a uniform cubic mesh with $N_g = 128^3$ grid points. There is then one particle per grid cell (on average) and the comoving separation between neighbouring grid points in the mesh is $\Delta = L/N_g^{1/3} = 1.5625h^{-1} \text{ Mpc}$, which is roughly the size of a typical galaxy group. At each output value of the scale factor, we use the comoving positions of the particles in the simulation to generate the CDM density field on the cubic mesh by applying triangular-shaped cloud interpolation (e.g. [30]). The three approximation methods we are comparing all use the linear growth factor D as a time variable, rather than the scale factor a . We therefore convert the output values of the scale factor used in the simulation to values of the linear growth factor by noting that, in a spatially-flat Λ CDM cosmology, the solution of (3) is

$$D \propto \frac{5}{6} \mathcal{B}_\alpha(5/6, 2/3) \left(\frac{\Omega_{c,0}}{\Omega_{\Lambda,0}a^3} \right)^{1/3} \left(1 + \frac{\Omega_{c,0}}{\Omega_{\Lambda,0}a^6} \right)^{1/2}, \quad (11)$$

where the constant of proportionality is chosen to ensure $D_i = 1$, \mathcal{B}_α is the incomplete beta function and $\alpha = \alpha(a)$ is defined by

$$\alpha = \frac{\Omega_{\Lambda,0}a^3}{\Omega_{c,0} + \Omega_{\Lambda,0}a^6}. \quad (12)$$

We now describe how the CDM density field can be calculated at any particular value of the linear growth factor for each of the approximation schemes we are considering.

The free-particle approximation. The first step is to determine the initial velocity potential ϕ_i on the cubic mesh. This is done by numerically solving $\nabla_{\mathbf{x}}^2 \phi_i = \delta_i$ in Fourier space, where δ_i is the initial CDM density field of the N -body simulation. The initial wavefunction ψ_i is generated on the mesh by inserting δ_i and ϕ_i into

$$\psi_i = (1 + \delta_i)^{1/2} \exp\left(\frac{-i\phi_i}{\nu}\right), \quad (13)$$

along with a suitable finite value of ν . We discuss how the optimal value of ν can be found in section 4.1. The discrete Fourier transform $\hat{\psi}_i = \hat{\psi}_i(\mathbf{k})$ of the initial wavefunction is then calculated and the exact solution of the free-particle Schrödinger equation (1):

$$\hat{\psi} = \hat{\psi}_i \exp\left[\frac{-i\nu(D-1)k^2}{2}\right] \quad (14)$$

is used to determine the Fourier transform $\hat{\psi} = \hat{\psi}(\mathbf{k}, D)$ of the wavefunction at any $D \geq 1$ of interest. Here \mathbf{k} is a comoving wavevector and $k = |\mathbf{k}|$. The wavefunction ψ in real space follows by taking the inverse discrete Fourier transform of $\hat{\psi}$ and the CDM density field is determined from the amplitude of the wavefunction via $\delta = |\psi|^2 - 1$. As we shall see in section 4, knowledge of the velocity potential ϕ is also useful. We calculate ϕ on the cubic mesh by using numerical Fourier techniques to solve (7).

The linearized fluid approach. The CDM density field δ at any $D \geq 1$ is determined from the initial N -body density field δ_i by simply applying the linear growth law $\delta = D\delta_i$.

The Zeldovich-Bernoulli approximation. The initial velocity potential ϕ_i is constructed on the cubic mesh as before and the Zeldovich-Bernoulli equation

$$\frac{\partial \phi}{\partial D} - \frac{1}{2} |\nabla_{\mathbf{x}} \phi|^2 = 0 \quad (15)$$

is integrated forwards in time from $D_i = 1$ to D_0 using the simple numerical scheme described in [24]. At each time step in the integration we know ϕ and so the CDM density field δ can be numerically calculated on the mesh via (7).

4. Results and discussion

In order to optimize the free-particle approximation, it is essential to select the parameter ν carefully. We briefly address this issue before proceeding to test the free-particle method against the linearized fluid and Zeldovich-Bernoulli approximations. First, we introduce a dimensionless parameter $\Gamma = \nu/\Delta^2$ with Δ defined as before. The parameter Γ emerges upon rewriting the free-particle Schrödinger equation (1) in terms of the dimensionless comoving coordinate $\bar{\mathbf{x}} = \mathbf{x}/\Delta$. Note that $\Gamma \propto \nu$; hereafter we will analyse the behaviour of the free-particle approximation in terms of Γ rather than ν .

4.1. Optimizing the free-particle approximation

The numerical implementation of the free-particle approximation described in section 3.2 requires a finite value of Γ , rather than $\Gamma \rightarrow 0$. Recall that, in this case, the quantum pressure term impedes the gravitational collapse of density perturbations even before multi-stream regions are formed. However, since $\mathcal{P} \propto \Gamma^2$, this undesirable effect can be minimized by choosing the smallest possible value of Γ . In order to find this optimal value of Γ , we first note that the phase of the initial wavefunction (13) is $\arg(\psi_i) = -\phi_i/\nu \propto 1/\Gamma$. Sampling the initial phase field at the Nyquist sampling rate requires that the change in phase between two adjacent grid points in the cubic mesh must be less than or equal to π radians. As Γ is decreased towards zero, the phase of the initial wavefunction varies increasingly rapidly and this condition will eventually be violated. Phase-aliasing effects then cause the power spectrum of the initial wavefunction ψ_i to become very noisy and our method breaks down. The optimal value of Γ , Γ_c , is then defined as the smallest value of Γ for which there is no phase-aliasing; we ensure there is no aliasing by using a simple numerical algorithm to check that the phase difference between each point in the mesh and its nearest neighbours is not greater than π radians. The value of Γ_c is mesh-dependent and, in the work presented here, $\Gamma_c = 0.12$. To illustrate that $\Gamma = \Gamma_c$ is indeed the optimal case, we compare the relative sizes of the quantum pressure \mathcal{P} and convective $\mathcal{C} = -|\nabla_{\mathbf{x}}\phi|^2/2$ terms in the Bernoulli equation (5) for several different choices of Γ . We do this by introducing a ratio $\chi = \chi(a)$, defined by $\chi = \langle |\mathcal{P}| \rangle / \langle |\mathcal{C}| \rangle$. For each value of Γ we also investigate how the quantum pressure term affects the formation of large-scale structure within the free-particle approximation.

Figure 1 shows how the ratio χ evolves with the scale factor. For the moment we focus on the three solid lines, corresponding to $\Gamma = 0.12$, $\Gamma = 0.6$ and $\Gamma = 20$, respectively. Observe that the ratio χ increases monotonically with the scale factor in all cases, implying that, on average, the quantum pressure grows relative to the convective term as time proceeds. We can also see that, at any particular value of the scale factor, the value of χ decreases as Γ is decreased. Therefore, on average, the quantum pressure term becomes less significant (relative to the convective term) as the value of Γ is made smaller. At each value of the scale factor, we find that the smallest value of χ is indeed obtained for $\Gamma = \Gamma_c = 0.12$. For reasons that will become clear in section 4.2, we also examine the behaviour of χ when the free-particle density field is smoothed with a Gaussian filter prior to calculating the quantum pressure and convective terms (note that we apply the smoothing first to ensure numerical gradients are well behaved). The dashed and dotted lines in figure 1 show how χ evolves for two smoothing scales: $r_{\text{sm}} = 4h^{-1}$ Mpc and $r_{\text{sm}} = 8h^{-1}$ Mpc, respectively. In both cases the value of χ is very small at all values of the scale factor and, as the smoothing length is increased, the quantum pressure term diminishes relative to the convective term (on average).

In figure 2 we show slices through the final (i.e. at $a = a_0 = 1$) N -body and free-

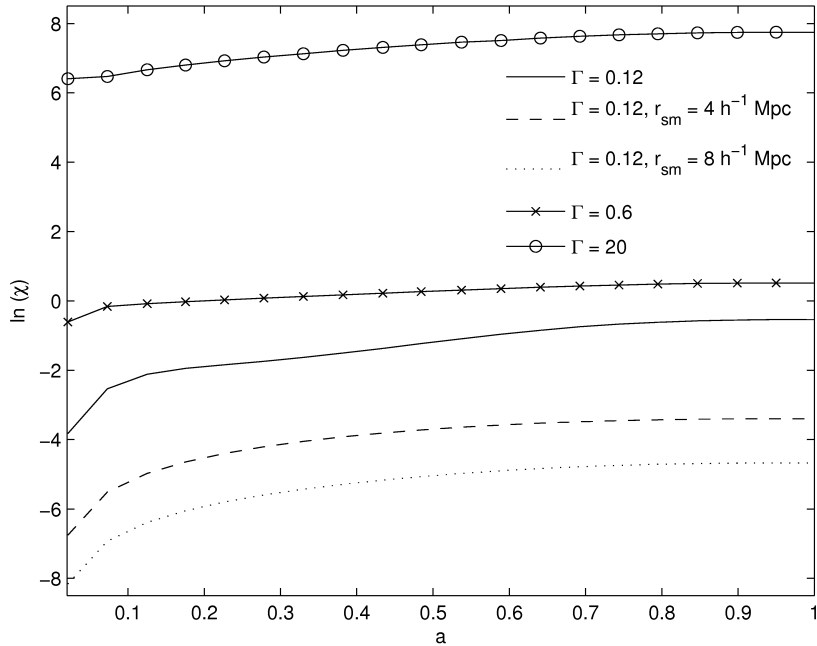


Figure 1. The ratio $\chi = \langle |\mathcal{P}| \rangle / \langle |\mathcal{C}| \rangle$ plotted as a function of the scale factor a for three different values of the parameter Γ . The dashed and dotted lines show how χ evolves when the free-particle (with $\Gamma = 0.12$) density field has been smoothed with Gaussian filters of radii $r_{\text{sm}} = 4h^{-1}$ Mpc and $r_{\text{sm}} = 8h^{-1}$ Mpc, respectively.

particle density fields for the cases $\Gamma = 0.12$, $\Gamma = 0.6$ and $\Gamma = 20$. The global morphology of the free-particle density field agrees well with that of the N -body density field for $\Gamma = 0.12$, with the peaks of the two density fields located at the same positions. However, the over-densities formed in the free-particle approximation are not as large as in the N -body simulation and the free-particle density field is considerably smoother than the N -body density field. This is not surprising since the free-particle approximation is essentially a quasi-linear method and thus cannot account for the full non-linear growth of density perturbations. As the value of Γ is increased to 0.6 the pattern of large-scale structure appears ‘smeared out’ in the free-particle approximation. This is because the quantum pressure term is now larger on average (see figure 1) and inhibits the collapse of density perturbations over a greater distance; see also [22]. Similar behaviour is also seen in the adhesion approximation as the viscosity parameter μ is increased [9]. In the case where $\Gamma = 20$, the quantum pressure term completely dominates the convective term on average (figure 1) and there is no growth of density fluctuations whatsoever. Instead, the initial density field simply oscillates rapidly in a seemingly random fashion and remains close to homogeneous. This oscillatory behaviour was also observed in the simple test of the free-particle approximation performed by Short and Coles [22].

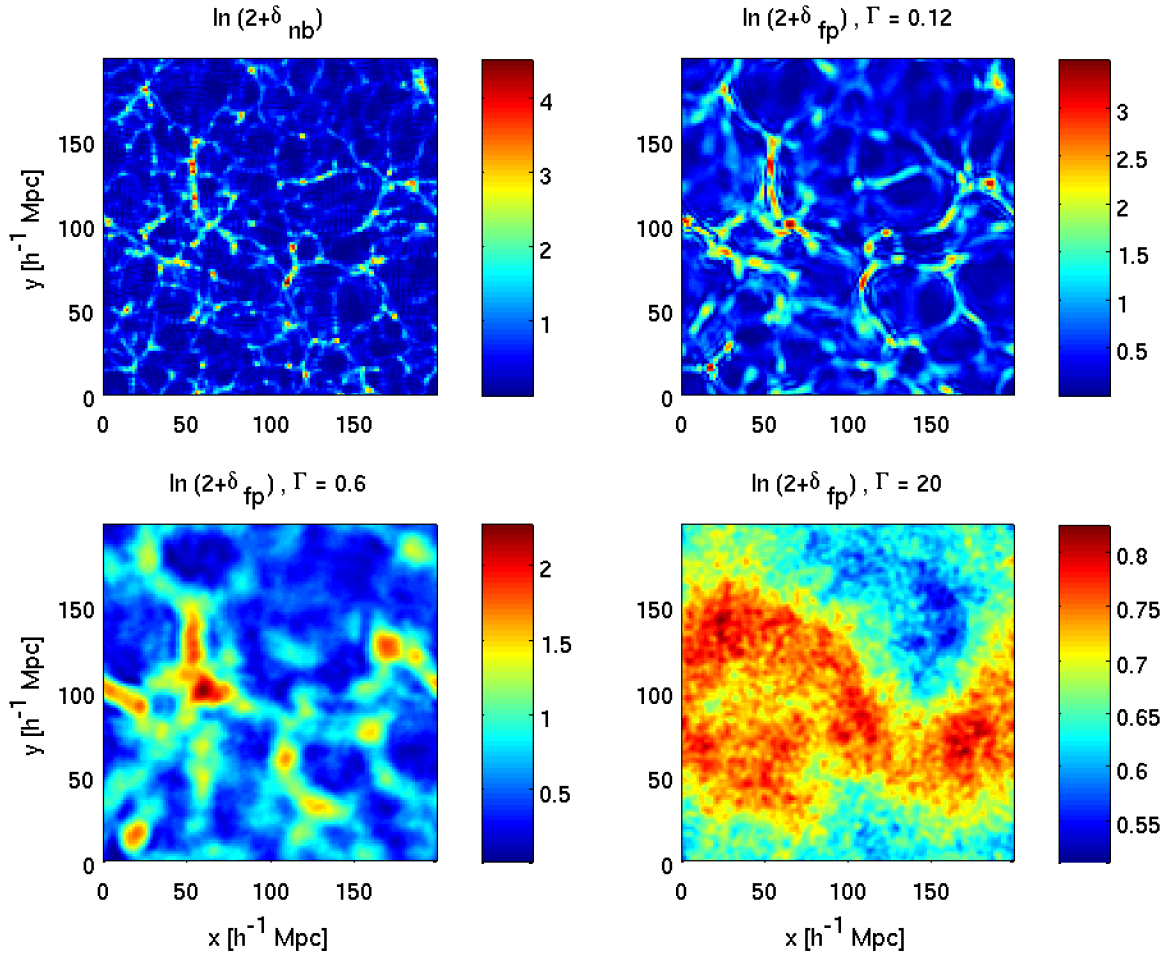


Figure 2. Slices through the N -body density field δ_{nb} and the free-particle density fields δ_{fp} for three different choices of the dimensionless parameter Γ . The value of the scale factor is $a = a_0 = 1$ and the slices are arbitrarily taken at a z -coordinate of $100h^{-1}$ Mpc.

4.2. Comparison of approximation schemes

We have established that our free-particle method will be optimized for $\Gamma = \Gamma_c = 0.12$. Accordingly, we set $\Gamma = 0.12$ in the free-particle approximation for the remainder of this work. We now use the method described in section 3.2 to test the free-particle approximation against an N -body simulation and compare our results with those of the linearized fluid approach and the Zeldovich-Bernoulli approximation.

Figure 3 shows point-by-point comparisons of the density fields obtained from the three approximation schemes with the N -body density field. If the density field δ obtained from any one of our approximation methods is identical to the N -body density field δ_{nb} at all points in the cubic mesh, then there will be no scatter about the diagonal line overlaid on each plot. We quantify any scatter about the diagonal by using the

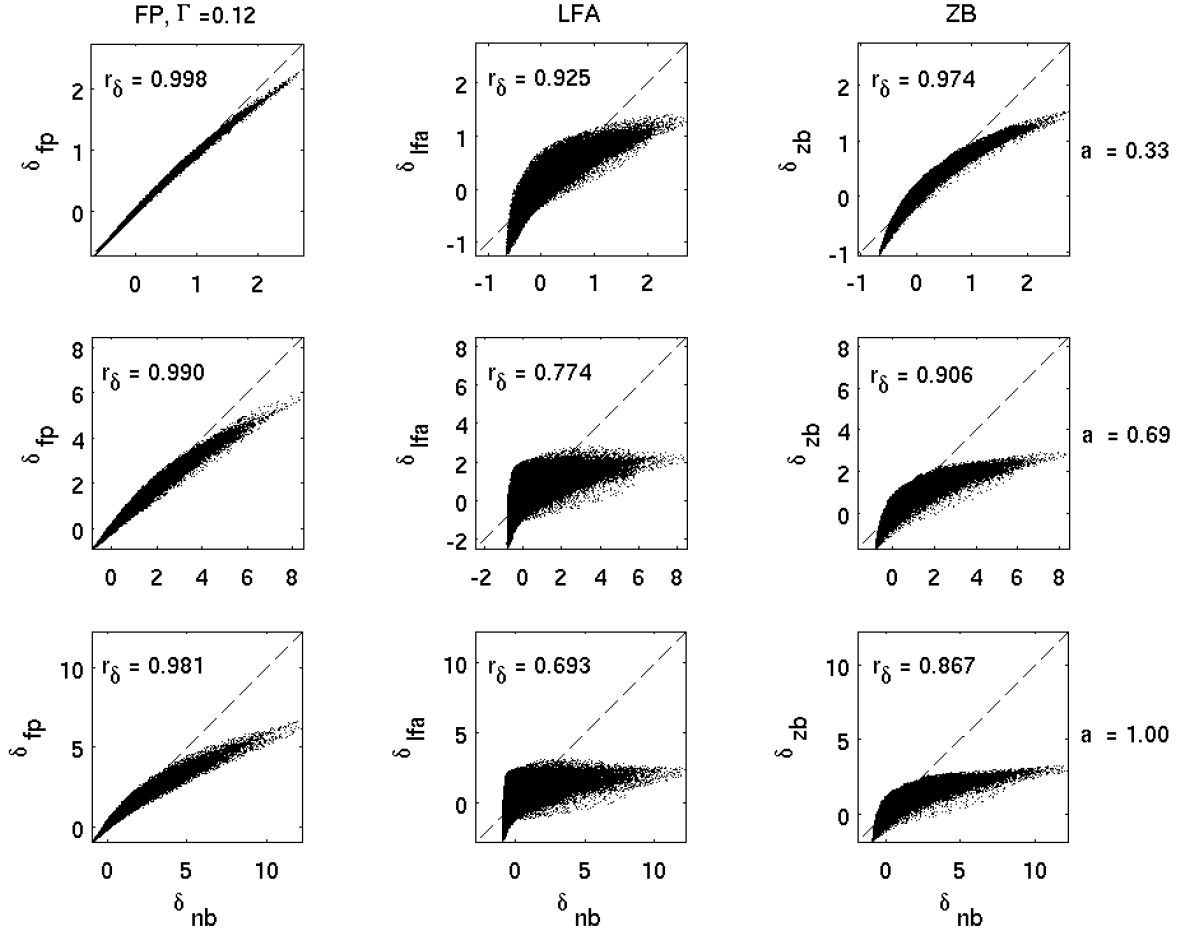


Figure 3. Point-by-point comparisons of the density fields obtained from the three approximation schemes and the N -body density field δ_{nb} . The first, second and third columns correspond to the free-particle (with $\Gamma = 0.12$), linearized fluid and Zeldovich-Bernoulli approximations, respectively. Comparisons are shown for three different values of the scale factor a and all of the density fields have been smoothed with a Gaussian filter of radius $r_{\text{sm}} = 4h^{-1}$ Mpc. The corresponding value of the correlation coefficient r_δ between the density fields is shown in the top-left corner of each plot.

correlation coefficient

$$r_\delta = \frac{\langle \delta_{\text{nb}} \delta \rangle}{\langle \delta_{\text{nb}}^2 \rangle^{1/2} \langle \delta^2 \rangle^{1/2}}; \quad (16)$$

a value of $r_\delta = 1$ corresponds to the case where there is no scatter. All of the density fields in figure 3 have been smoothed with a Gaussian filter of radius $r_{\text{sm}} = 4h^{-1}$ Mpc to smooth over highly non-linear regions where the linear/quasi-linear approximation methods we are testing cannot be expected to give reliable results. The main result of figure 3 is that the free-particle approximation performs significantly better than both the linearized fluid and Zeldovich-Bernoulli approximations when tested against an N -body simulation. It is clear from the point-by-point comparisons that, at any given value of the scale factor, the free-particle density field displays the best correlation with

the N -body density field. Observe that the extrapolation of first-order Eulerian and Lagrangian perturbation theory to late times leads to unphysical regions in the density field where $\delta < -1$, i.e. where $\rho < 0$. This problem is neatly side-stepped in the free-particle approximation since, by definition, $\delta = |\psi|^2 - 1$ and $|\psi|^2 \geq 0$. This explains why the free-particle density field provides the best match to the N -body density field in low density regions. It is evident from figure 3 that, even after applying smoothing, all of the approximation methods systematically underestimate the density in high-density regions. However, it is interesting to note that the free-particle approximation performs considerably better than the other approximation methods in high density regions too.

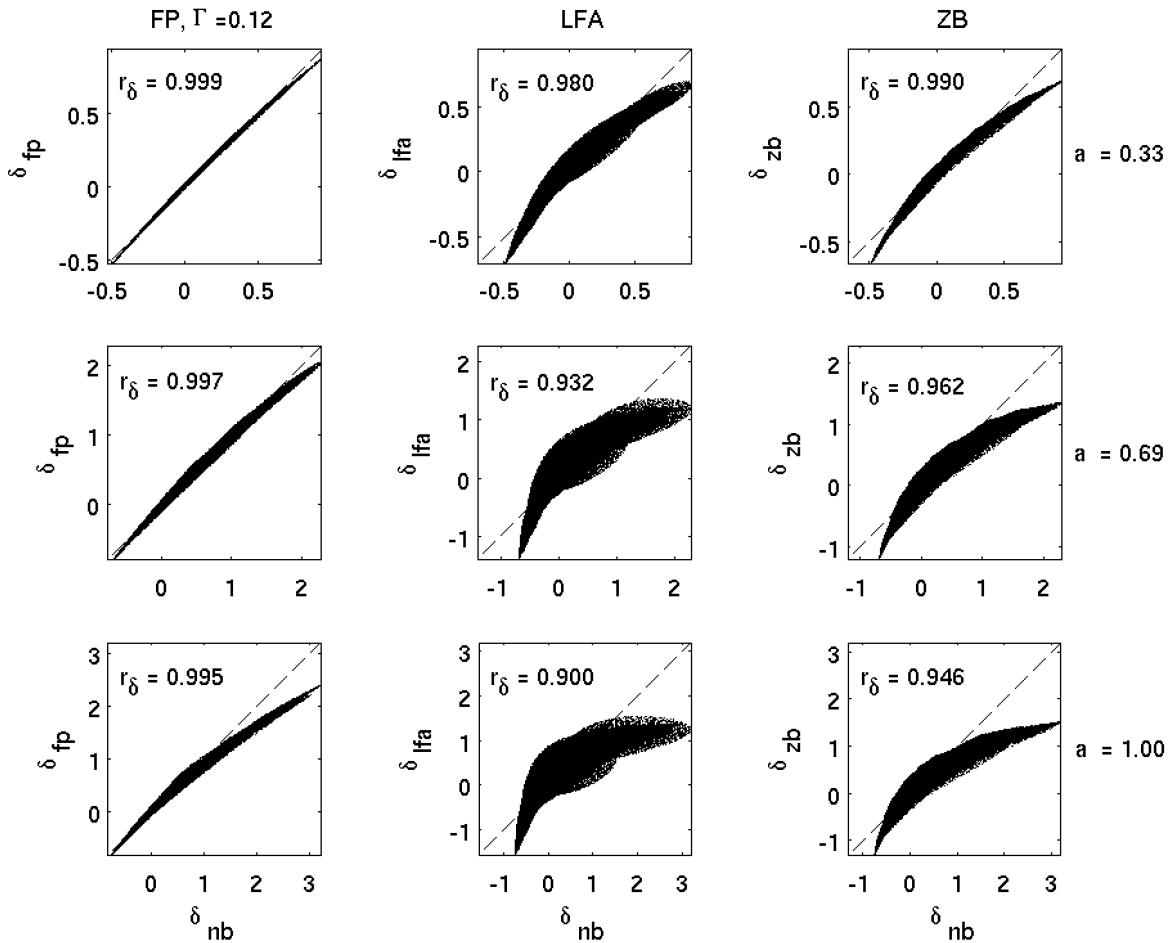


Figure 4. Point-by-point comparisons of the density fields obtained from the three approximation schemes and the N -body density field δ_{nb} . The layout of the plots is the same as in figure 4; the only difference is that all of the density fields have been smoothed with a Gaussian filter of radius $r_{\text{sm}} = 8h^{-1}$ Mpc.

Figure 4 is essentially the same as figure 3 except that all of the density fields have been smoothed with a Gaussian filter of radius $r_{\text{sm}} = 8h^{-1}$ Mpc. By using a larger smoothing scale we restrict all of the density fields to the quasi-linear regime $\delta \sim 1$. Consequently, the performance of all the approximation methods is improved. However, the free-particle approximation still clearly out-performs the linearized fluid

and Zeldovich-Bernoulli approximations. The correlation between the smoothed free-particle and N -body density fields is very good at all values of the scale factor, with only a slight discrepancy between the two density fields in high-density regions as $a \rightarrow 1$. Although the smoothing is now much heavier, the linearized fluid approach and the Zeldovich-Bernoulli approximation still generate negative matter densities at late times.

The correlation coefficient r_δ provides a simple way of quantifying the scatter about the diagonal in the point-by-point comparisons of figure 3 and figure 4. In figure 5 we explicitly plot r_δ as a function of the scale factor for each approximation scheme. Results are shown for the two smoothing scales: $r_{\text{sm}} = 4h^{-1}$ Mpc and $r_{\text{sm}} = 8h^{-1}$ Mpc. It is immediately clear that, for both smoothing lengths, the free-particle approximation consistently yields a higher value of r_δ than the other two methods. It is interesting to note that, when the free-particle density field is smoothed with a Gaussian filter of radius $r_{\text{sm}} = 4h^{-1}$ Mpc, the value of r_δ obtained is always larger than that calculated from the linearized fluid and Zeldovich-Bernoulli density fields smoothed on a scale of $8h^{-1}$ Mpc. In other words, even when the linearized fluid and Zeldovich-Bernoulli density fields are more heavily smoothed, the correlation with the N -body density field is still not as good.

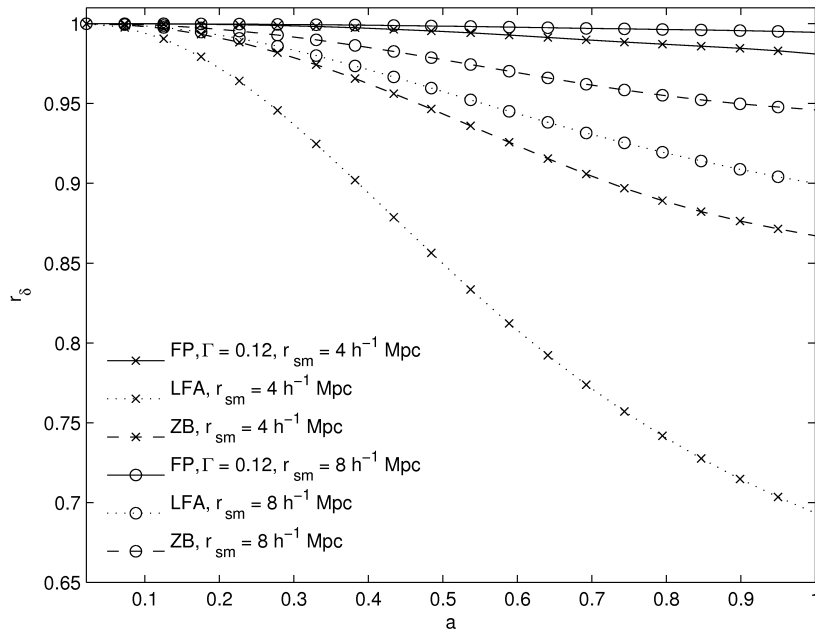


Figure 5. The correlation coefficient r_δ for each of the three approximation schemes plotted as a function of the scale factor a . Results are shown for the two smoothing lengths $r_{\text{sm}} = 4h^{-1}$ Mpc and $r_{\text{sm}} = 8h^{-1}$ Mpc.

A simple means of examining the statistical properties of the density fields in the different approximation schemes is afforded by the one-point probability distribution function (PDF) $P_\delta = P_\delta(\delta)$ of the density fields. The PDF of the initial N -body density field is Gaussian by construction. However, non-linear gravitational evolution causes the N -body PDF to become non-Gaussian at late times. The distribution becomes skewed

since positive density fluctuations (over-densities) can grow indefinitely whereas negative density fluctuations (under-densities) cannot exceed $\delta = -1$. Figure 6 shows the PDFs of the various density fields at the final time $a = a_0 = 1$ for the smoothing lengths $r_{\text{sm}} = 4h^{-1}$ Mpc and $r_{\text{sm}} = 8h^{-1}$ Mpc. The corresponding PDFs of the N -body density field are shown for reference. We can see that, for both smoothing scales, the PDF of the free-particle density field provides the best match to the N -body PDF for all values of δ . The fact that the free-particle approximation guarantees $\delta \geq -1$ causes the free-particle PDF to be skewed in the same way as the N -body PDF. It is clear from both plots in figure 6 that the PDF of the linearized fluid density field is Gaussian. This must be the case for Gaussian initial conditions since the density contrast at a given point simply grows proportional to the linear growth factor to first-order in Eulerian perturbation theory. The PDFs of the Zeldovich-Bernoulli density field also seem to be close to Gaussian. Consequently, the linearized fluid and Zeldovich-Bernoulli approximations both assign a non-zero probability to the existence of regions with $\delta < -1$ at late times.

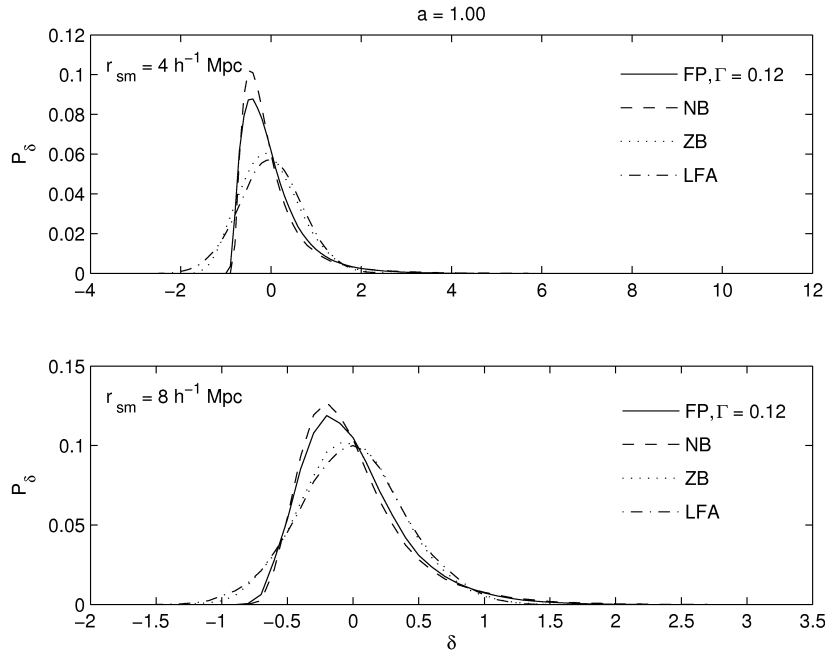


Figure 6. The one-point PDFs P_δ of the density fields obtained from the free-particle (with $\Gamma = 0.12$), linearized fluid and Zeldovich-Bernoulli approximations. The N -body PDFs are also shown for comparative purposes. The value of the scale factor is $a = a_0 = 1$ and the top and bottom plots correspond to the smoothing lengths $r_{\text{sm}} = 4h^{-1}$ Mpc and $r_{\text{sm}} = 8h^{-1}$ Mpc, respectively.

In our discussion so far we have only compared the performance of the free-particle, linearized fluid and Zeldovich-Bernoulli approximations in real space. However, it is informative to examine the behaviour of the different approximation schemes in Fourier space as well. For each method we investigate how the Fourier components $\hat{\delta} = \hat{\delta}(\mathbf{k}, a)$ of the appropriate density field evolve relative to the corresponding Fourier components $\hat{\delta}_{\text{nb}} = \hat{\delta}_{\text{nb}}(\mathbf{k}, a)$ of the N -body density field. To do this we use the statistic $\epsilon = \epsilon(k, a)$,

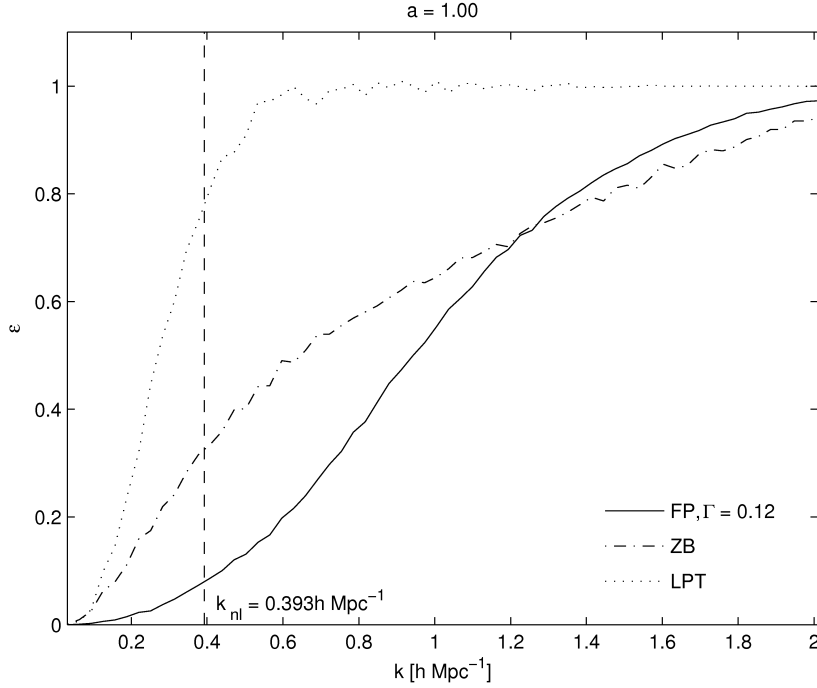


Figure 7. The statistic ϵ plotted as a function of the comoving wavenumber k for each of the three approximation schemes. The value of the scale factor is $a = a_0 = 1$. The dashed vertical line corresponds to the wavenumber $k_{\text{nl}} = 0.3927h \text{ Mpc}^{-1}$ which indicates the boundary between Fourier modes in the linear and non-linear regimes.

defined by

$$\epsilon = \frac{\sum |\hat{\delta} - \hat{\delta}_{\text{nb}}|^2}{\sum (|\hat{\delta}|^2 + |\hat{\delta}_{\text{nb}}|^2)}, \quad (17)$$

where, for each (comoving) wavenumber k , the summations are over all wavevectors \mathbf{k} with a magnitude in the interval $(k - 2\pi/L, k]$. The quantity ϵ provides a measure of the differences between the amplitudes and phases of the Fourier components $\hat{\delta}$ and $\hat{\delta}_{\text{nb}}$. If the amplitudes and phases of the Fourier components of the two fields are identical then $\epsilon = 0$. On the contrary, if the phases of the two fields are completely uncorrelated then $\epsilon = 1$ on average. A convenient property of the statistic ϵ is that it is independent of any smoothing of the density fields and so we are free to use the un-smoothed density fields to calculate ϵ . Figure 7 shows ϵ as a function of the wavenumber k at the final time $a = a_0 = 1$ for the different approximation schemes we are considering. The vertical dashed line shown in the plot denotes the wavenumber $k_{\text{nl}} = 0.3927h \text{ Mpc}^{-1}$ which corresponds to a wavelength of $\lambda_{k_{\text{nl}}} = 16h^{-1} \text{ Mpc}$. From observations, the present rms density fluctuation in spheres of diameter $\lambda_{k_{\text{nl}}}$ is of order unity and so the scale k_{nl} can be taken as an indication of the boundary between modes in the linear and non-linear regimes of gravitational evolution. Fourier modes with a wavenumber $k < k_{\text{nl}}$ are still in the linear regime and evolve independently of each other. The phase information of the initial density field is preserved in this case. On the other hand, modes with a

wavenumber $k \geq k_{\text{nl}}$ experience phase shifts due to coupling between different modes in the non-linear regime (e.g. [31, 32]). It is apparent from figure 7 that, for all of the approximation schemes, the value of ϵ becomes larger as k is increased. This is not surprising since the various methods we are comparing cannot accurately follow the non-linear evolution of small-scale modes. The main point of figure 7 is that, for wavenumbers in the range $0 < k \lesssim 3k_{\text{nl}}$, the value of ϵ is consistently smaller in the free-particle approximation than in the linearized fluid and Zeldovich-Bernoulli approximations. In particular, the free-particle approximation performs much better than the other two methods for $0 < k < k_{\text{nl}}$. Notice that the Zeldovich-Bernoulli approximation gives a slightly lower value of ϵ than the free-particle approximation for $k \gtrsim 3k_{\text{nl}}$. However, the wavenumber $k = 3k_{\text{nl}}$ corresponds to a wavelength $\lambda_{3k_{\text{nl}}} = 5.3333h^{-1}$ Mpc and we find that the rms density fluctuation in spheres of diameter $\lambda_{3k_{\text{nl}}}$ is approximately 2 for the final N -body density field. Thus we cannot realistically expect the free-particle and Zeldovich-Bernoulli approximations to yield reliable results on scales much smaller than this anyway.

5. Conclusion

In this paper we have investigated a new approach to the study of cosmological structure formation known as the free-particle approximation. The free-particle approximation is similar in spirit to the adhesion approximation in the sense that it is an extension of the Zeldovich approximation which includes a regularizing term - the quantum pressure term - to prevent the formation of density singularities when shell-crossing occurs. The quantum pressure is controlled by a free parameter ν (or Γ in the notation of section 4) which is akin to the viscosity coefficient μ in the adhesion model. In the semi-classical limit $\nu \rightarrow 0$ the quantum pressure only has an effect in multi-stream regions. However, in this work we have employed a numerical implementation of the free-particle approximation that uses a finite value of ν instead. In this case the quantum pressure term acts to suppress the collapse of density perturbations away from regions where particle trajectories cross; the degree of suppression increases with ν .

The free-particle method has been rigorously tested by appealing to a full cosmological N -body simulation. We have shown that the performance of the free-particle approximation, relative to the N -body simulation, is optimized when ν is set to the smallest possible value ν_c supported by the discrete mesh we use. In this case the effect of the quantum pressure is minimal. For larger values of $\nu > \nu_c$ the quantum pressure term becomes more significant relative to the convective term in (5) and the details of the large-scale structure distribution appear ‘washed out’ in the free-particle approximation. In particular, for $\nu \gg \nu_c$, the quantum pressure term is dominant and initial density fluctuations undergo oscillation rather than growth. The free-particle approximation (with $\nu = \nu_c$) consistently yields better results than the established linearized fluid and Zeldovich-Bernoulli approximations in all of the tests discussed in section 4. At all times the density field obtained from the free-particle method is

considerably better correlated with the N -body density field than the density fields of the other two approximation schemes. This is particularly true in low density regions which is a consequence of the fact that the free-particle density field is guaranteed to be non-negative. This feature of the free-particle approximation also explains why the one-point PDF of the free-particle density field provides the closest match to the N -body PDF of all the approximation methods. We have also seen that the free-particle approximation out-performs the linearized fluid approach and the Zeldovich-Bernoulli approximation in Fourier space. From a practical point of view, another advantage of the free-particle approximation is that it is very quick to implement. This is because the free-particle Schrödinger equation has an exact solution, allowing us to directly calculate the density and velocity fields at any given time without having to numerically integrate equations of motion.

To conclude, the free-particle approximation provides a quick and effective way of evolving cosmological density perturbations into the quasi-linear regime in any CDM-dominated cosmology. We have compared the free-particle method with two traditional approaches and the results have proved favourable. In light of these comments, we believe that the free-particle approximation provides another useful addition to the repertoire of analytical techniques available for the study of large-scale structure formation.

Acknowledgments

C J Short would like to thank PPARC for the award of a studentship that made this work possible. Also, we are grateful to F R Pearce for many useful comments regarding numerical issues and to the anonymous referee for helpful suggestions.

References

- [1] Coles P 2005 *Nature* **433** 248
- [2] Sahni V and Coles P 1995 *Phys. Rep.* **262** 1
- [3] Bernardeau F, Colombi S, Gaztanaga E and Scoccimarro R 2002 *Phys. Rep.* **367** 1
- [4] Peebles P J E 1980 *The Large-scale Structure of the Universe* (Princeton University Press)
- [5] Zeldovich Ya B 1970 *Astron. Astrophys.* **5** 84
- [6] Coles P, Melott A L and Shandarin S F 1993 *Mon. Not. R. Astron. Soc.* **260** 765
- [7] Gurbatov S N, Saichev A I and Shandarin S F 1989 *Mon. Not. R. Astron. Soc.* **236** 385
- [8] Kofman L, Pogosyan D and Shandarin S F 1990 *Mon. Not. R. Astron. Soc.* **242** 200
- [9] Weinberg D H and Gunn J E 1990 *Mon. Not. R. Astron. Soc.* **247** 260
- [10] Nusser A and Dekel A 1990 *Astrophys. J.* **362** 14
- [11] Kofman L, Pogosyan D, Shandarin S F and Melott A L 1992 *Astrophys. J.* **393** 437
- [12] Melott A L, Shandarin S F and Weinberg D H 1994 *Astrophys. J.* **428** 28
- [13] Buchert T and Domínguez A 1998 *Astron. Astrophys.* **335** 395
- [14] Buchert T, Domínguez A and Pérez-Mercader J 1999 *Astron. Astrophys.* **349** 343
- [15] Domínguez A 2000 *Phys. Rev. D* **62** 103501
- [16] Domínguez A 2002 *Mon. Not. R. Astron. Soc.* **334** 435
- [17] Buchert T and Domínguez A 2005 *Astron. Astrophys.* **438** 443

- [18] Widrow L M and Kaiser N 1993 *Astrophys. J.* **416** L71
- [19] Widrow L M 1997 *Phys. Rev. D* **55** 10
- [20] Coles P 2002 *Mon. Not. R. Astron. Soc.* **330** 421
- [21] Coles P and Spencer K 2003 *Mon. Not. R. Astron. Soc.* **342** 176
- [22] Short C J and Coles P 2006 *Preprint* astro-ph/0605012
- [23] Madelung E 1926 *Zts. f. Phys.* **40** 322
- [24] Nusser A and Dekel A 1992 *Astrophys. J.* **391** 443
- [25] Burgers J M 1940 *Proc. R. Neth. Acad. Sci.* **43** 2
- [26] Sahni V, Sathyaprakash B S and Shandarin S F 1994 *Astrophys. J.* **431** 20
- [27] Couchman H M P, Thomas P A and Pearce F R 1995 *Astrophys. J.* **452** 797
- [28] Brandenberger R H 1985 *Rev. Mod. Phys.* **57** 1
- [29] Bardeen J M, Bond J R, Kaiser N and Szalay A S 1986 *Astrophys. J.* **304** 15
- [30] Hockney R W and Eastwood J W 1988 *Computer Simulation Using Particles* (Institute of Physics Publishing)
- [31] Ryden B and Gramman M 1991 *Astrophys. J.* **383** L33
- [32] Chiang L Y and Coles P 2000 *Mon. Not. R. Astron. Soc.* **311** 809